Molecular Resolution Imaging of Macromolecular Crystals by Atomic Force Microscopy

Yu. G. Kuznetsov,* A. J. Malkin,* T. A. Land,# J. J. DeYoreo,# A. P. Barba,* John Konnert,§ and A. McPherson*

*Department of Biochemistry, University of California, Riverside, Riverside, California 92521; #Department of Chemistry and Materials Science, Lawrence Livermore National Laboratory, Livermore, CA 94550; and §Laboratory for the Structure of Matter, Naval Research Laboratory, Washington, DC 20375 USA

ABSTRACT Atomic force microscopy (AFM) images at the molecular level have been obtained for a number of different protein and virus crystals. They can be utilized in some special cases to obtain information useful to crystal structure analyses by x-ray diffraction. In particular, questions of space group enantiomer, the packing of molecules within a unit cell, the number of molecules per asymmetric unit, and the dispositions of multiple molecules within the asymmetric unit may be resolved. In addition, because of the increasing sensitivity and resolution of the AFM technique, some molecular features of very large asymmetric units may be within reach. We describe here high-resolution studies, using AFM, to visualize individual molecules and viruses in their crystal lattices. These investigations included fungal lipase, lysozyme, thaumatin, canavalin, and satellite tobacco mosaic virus (STMV).

INTRODUCTION

Since the first demonstration by Durbin that the method of atomic force microscopy could be profitably applied to the examination of protein crystal growth (Durbin and Carlson, 1992; Durbin et al., 1993), a number of laboratories, including our own, have taken advantage of AFM to investigate the mechanisms of macromolecular crystal growth and the many phenomena associated with that process (Konnert et al., 1994; Malkin et al., 1995a,b, 1996a,b,c; Yip and Ward, 1996; Land et al., 1995). As these studies progressed, improvements in the methods resulted in enhanced quality and resolution of images. It is now often possible to directly visualize individual macromolecules, both proteins and viruses, on the surfaces of growing crystals.

A number of features of AFM make this a significant development for protein crystallographers. The kind of information found in AFM images is clearly different from that available from other microscopies, such as transmission electron microscopy. First of all, AFM images are obtained from macromolecular crystals in situ, that is, as they exist in their mother liquor, and even while they are still growing, without any observable perturbation to the crystals or the growth process (Durbin and Carlson, 1992). Thus there is no dehydration of the crystals and the lattice is observed as it would be during the course of an x-ray diffraction experiment. There is no need for fixatives because the AFM tip exerts an insignificant force on the sample, and no need for extraneous molecules such as dyes or heavy atom stain, because contrast is provided by the topology of features and difference in height of points on the sample surface.

A second and particularly useful property of AFM images is that unlike transmission electron micrographs, they are not projections of the entire sample onto a single plane, but contain three-dimensional information. Thus the handedness of objects is retained in AFM images, including those of macromolecular crystals, and estimates of all three components of translational relationships can be obtained for molecules within the unit cell.

A third intriguing feature is that whereas all asymmetric units (generally one macromolecule) are crystallographically equivalent in the interior of a crystal, and therefore have identical chemical and physical environments, this is not true of molecules on the surface of a crystal. On the surface of a crystal, each molecule is distinct and exhibits a molecular orientation different from that of other (eventually crystallographically equivalent) molecules within a unit cell. Thus an AFM image of a crystal surface will, in general, simultaneously present multiple, symmetrically related perspectives on a single object, the molecule, thus providing three-dimensional visual information. This advantage can be extended if AFM images are obtained from more than one noncrystallographically equivalent face of the crystal.

We would like to present here AFM images of several different macromolecular crystals; lipase, thaumatin, canavalin, lysozyme, and satellite tobacco mosaic virus, with the intention of illustrating how the information they contain might be of value in broader structural studies, particularly x-ray crystallography. Although our attempts are somewhat rudimentary at this stage, it should be borne in mind that the full potential of the AFM technique has by no means been fully realized. Increases in sensitivity and resolution are the common expectation, reasonably so, and with them comes an enhanced role in structure determination.

Received for publication 19 July 1996 and in final form 31 January 1997.

Address reprint requests to Dr. Alexander McPherson, Department of Biochemistry, University of California, Room 2466, Boyce Hall, Riverside, CA 92521. Tel.: 909-787-5391; Fax: 909-787-3790; E-mail: mcpherson@ucrac1.ucr.edu.

0006-3495/97/05/2357/08 $2.00

MATERIALS AND METHODS

Thaumatin from *Thaumatococus danielli* (Ko et al., 1994) and hen egg lysozyme (Alderton and Fevold, 1946) were purchased from Sigma Biochemical Co. The fungal lipase (Derewenda et al., 1992) was a gift of Novo-Nordisk Co. (Copenhagen, Denmark). Canavalin and satellite tobacco mosaic virus (STMV) were prepared as previously described from (for canavalin) Jack Bean meal purchased from Sigma (Ng et al., 1993; Ko et al., 1993a,b) and (for STMV) from tobacco leaves coinfected with STMV and its helper virus TMV (Koszelak et al., 1989; Larson et al., 1993). Although the proteins and their structures are described in more detail elsewhere, some relevant molecular properties are presented in Table 1.

Crystallization conditions for each protein or virus presented in Table 1 assume a standard vapor diffusion arrangement in which the initial concentration of precipitant in the droplet of mother liquor is initially half that of the reservoir and is attained by mixing equal volumes of a protein stock solution with the reservoir solution. All crystal growth experiments and analyses described here were carried out at room temperature. The protein stock solutions, depending on the ultimate supersaturation required, were 1) canavalin (15–30 mg/ml), 2) lysozyme (25–50 mg/ml), 3) thaumatin (10–30 mg/ml), 4) lipase (4–10 mg/ml), and 5) STMV (2–8 mg/ml). The areas of the surfaces of the crystals examined in the AFM ranged from those as small as 50 μm^2 to, in some cases, final sizes greater than 0.5 mm^2.

A major problem in imaging macromolecular crystals with atomic force microscopy is obtaining samples that are secured to some substrate, such as glass, so that they do not move during the course of scanning. If firmly fixed, then an area, or many different areas, on the crystals' surfaces may be scanned over a period of many days. We have not yet identified an effective adhesive for protein crystals; thus we are compelled to immobilize the crystals by growing them directly on a substrate material that can then be inserted directly into the AFM fluid cell. This cylindrical chamber has a diameter of 6 mm and a slightly variable height, which accepts volumes of 50–80 μl.

Although the substrates may be of almost any material, we have usually used either nickel- or gold-plated electron microscopy grids glued to clean glass slips, and clean glass slips alone. Nucleation was achieved by depositing a 3–5-μl droplet of mother liquor on the substrate and placing it in a 35-mm-diameter petri dish, atop some support, where it could equilibrate against a reservoir solution of several milliliters, essentially by conventional vapor diffusion (McPherson, 1982). In some cases, as with lysozyme and thaumatin, nucleation was achieved by simple batch technique and no equilibration was required. Because of the small drop size, nucleation generally occurred in a few hours' time. As soon as crystals of 50 μm^2 or larger were observed to grow on the substrate, the substrate and its droplet were immediately transferred to the AFM liquid sample chamber, and the chamber flooded with 80 μl of a protein-containing mother liquor at a specified supersaturation. The crystallization solution, because of mixing, was sometimes unstable for as much as several hours. During this initial period fluid fluctuations resulting in poor images made recording difficult. Recording of AFM images was initiated as soon as the mother liquor stabilized.

Vapor diffusion procedures were carried out at room temperature, and visual observations made using an Olympus SZH microscope with a zoom lens system that provided magnifications of 7.5× to 64×. After insertion of the crystal-bearing substrate into the liquid chamber, it came under observation by a second optical microscope system (Nikon, Optizoom), which is integrated into the AFM instrument. Crystals were selected according to their orientation and quality by optical inspection, and the AFM stylus was placed on a chosen point on the surface of the crystal. This operation could be repeated as often as necessary to identify optimal areas for study.

A single crystal may provide only one, sometimes two, crystal surfaces for investigation, because those examined must be more or less horizontal. In general, however, there are usually multiple, sometimes many crystals on the substrate, and these usually exhibit a variety of different faces. Analyzing multiple crystals at a fixed supersaturation in a single drop can provide a multifaceted picture of the crystal lattice.

Because the crystals used here have distinctive morphologies, the particular crystal face under investigation usually can be identified by optical examination. In addition, the crystals are fully hydrated and in a native state during scanning, so that scale is preserved and distances, both periodic and otherwise, can be measured directly from the images (see Fig. 1). When major faces (100, 010, 001) are examined, cell dimensions can be

TABLE 1 Relevant molecular and crystallization properties

Protein	Source	Mol. wt.	Oligomer state	Size and shape	Crystal parameters	Mol. unit cell	Mol. asym. unit	Crystal growth conditions	Reference
Canavalin	Jack Bean (*Canavalis ensiformis*)	147,000	Trimer of identical subunits of 48,000	Flat cylinder (height 50 Å diameter 90 Å)	Rhombohedral ($a = b = c = 83$ Å equivalent hexagonal $a = b = 136.8$ Å $c = 75.7$ Å space group R3)	1 per rhombohedral cell	1/3	From Dulbecco's phosphate-buffered saline, pH 6.8	Ko et al., 1993a, b; Ng et al., 1993
Lysozyme	Hen egg white	14,500	Monomer	Ellipsoid (20 Å × 20 Å × 35 Å)	Tetragonal ($a = b =$ 37.9 Å $c = 79.1$ Å space group $P4_3\,2_12$)	8	1	From 3% NaCl in 0.1 M sodium acetate, pH 4.6	Alderton and Fevold, 1946
Thaumatin	Serendipity berry (*Thaumatococus danielli*)	21,500	Monomer	Roughly spherical (diam. 30–35 Å)	Tetragonal $a = b =$ 58.6 $c = 151.8$ space group $P4_12_12$)	8	1	From 1.6 M sodium-potassium tartrate in 0.1 M ADA buffer, pH 6.8	Ko et al., 1994
Lipase	Fungus	41,000	Monomer	Ellipsoidal (30 Å × 35 Å × 45 Å)	Hexagonal $a = b =$ 142.9 Å $c = 80.4$ Å space group $P6_1$ or $P6_5$)	12	2	From 0.4 M to 1.09 M sodium phosphate, pH	Derewenda et al., 1992
Satellite tobacco mosaic virus	Tobacco (*Nicotia tobaccum*)	1,450,000	Icosahedron of 60 identical subunits of 14,500	Spherical (diam. 170 Å)	Cubic $a = b = c =$ 257 Å space group P23)	4 virions	20 subunits	From 10% to 20% sat. ammonium sulfate	Koszelak et al., 1989; Larson et al., 1993

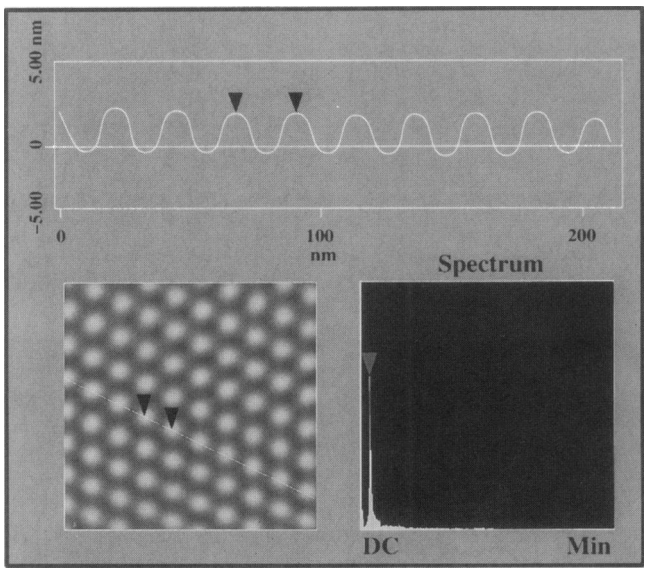

FIGURE 1 At lower left is a Fourier-filtered image of an area (190 × 190 nm^2) on the surface of an STMV crystal. The line drawn along a row of virus particles is reproduced at the top, with height variation added, showing, in turn, the periodicity of the surface. The two daggers can be specified by the AFM operator and distances immediately displayed. The power spectrum of the periodic array is shown at the lower right.

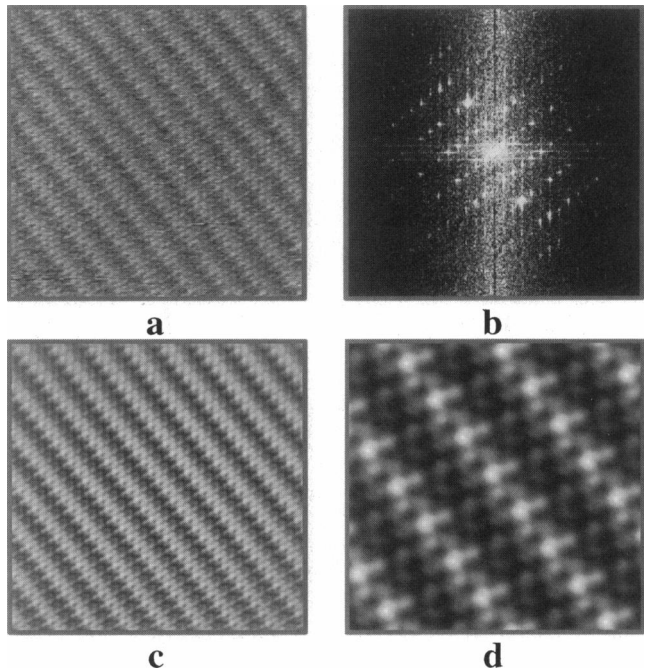

FIGURE 2 (*a*) A 200 × 200 nm^2 scan area image of the (100) face of a hexagonal crystal of fungal lipase, with space group $P6_1$ (or $P6_5$) and cell dimensions $a = b = 142.9$ Å, and $c = 80.4$ Å. The lattice, and even individual molecules, are clearly evident in this raw image. (*b*) Fourier transform (diffraction pattern) of the raw image, with a resolution of ~12–14 Å. It was subsequently filtered using the program ICE, and the Fourier-filtered image obtained from *a* is presented in *c*. (*d*) Fourier-filtered image (5 × 5 unit cells) of the lipase crystal. Light features are above and dark features below the mean plane of the crystal surface.

obtained directly from the images. Lateral resolution of nonperiodic features is about 15%, but for periodic features the Fourier transform provides accuracies of about 1–2%. Height measurements, on the other hand, are very sensitive, and deflections can be measured to within 0.2–0.3 nm.

In our experiments a J scanner on a Digital Nanoscope E atomic force microscope (Digital Instruments, Santa Barbara, CA) was used, allowing scan areas to vary from tens of nanometers up to more than a hundred microns. Both silicon nitride and oxide sharpened silicon nitride cantilevers (Digital Instruments) with a spring constant of 0.06 N/m were used as well as microlevers (Park Scientific, Sunnyvale, CA) with a spring constant of 0.01 N/m. Forces of 0.3 nN or less were typically applied.

When scanning, care was taken to continually adjust the set-point voltage to the lowest value for which tip-crystal contact was maintained, to minimize the force applied to the crystalline surface. However, some crystals, for example, those of turnip yellow mosaic virus, were so soft that application of even low force resulted in scarring of crystalline surfaces and, consequently, very poor AFM images. Thus one of the principal determinants of image quality for macromolecular crystals is crystal stiffness, and this varies from one macromolecule to another. Lysozyme and thaumatin crystals have excellent properties, whereas canavalin, for example, is softer. In cases where the crystals are physically well coupled to the substrate and are immobilized, where the growth rates are kept low by establishment of reduced supersaturation, and when macromolecular crystals are relatively mechanically hard, then the high-resolution AFM images presented here are quite representative of those that can be reproducibly obtained scan after scan.

To simulate the packing of molecules in the various unit cells, two programs were employed. In the simplest case, using a PC-based program, ATOMS (Shekunov), macromolecules were represented as spheres of a specified diameter. One molecule was assigned a position based on the AFM image or on x-ray crystallography results, and the remaining molecules in the unit cell were generated by applying space group operators. This, along with the cell dimensions, known from x-ray studies or measured from AFM images, permitted simulation of potential surface layers of the crystal. The chief advantage of this procedure, in addition to its simplicity, was that it clarified the dispositions of the various molecules on the surface.

Simulations on an SGI 340 VGX (as seen in Fig. 8 *a*), produced with the procedures of Konnert et al. (1994), are considerably more sophisticated. The actual shape of the macromolecule, based on its x-ray crystallographic structure, is re-created at a specified resolution and placed appropriately in the unit cell. The contents of the unit cell, generated from symmetry, with all molecules displayed in their proper orientations, is created and extended to produce the crystal surface. The expected AFM image is then generated by simulated scanning of an AFM probe with a 400-Å radius tip over the computed surface. The experimentally obtained AFM image can then be compared directly with the simulated AFM image. These procedures have been described in detail as applied to the principal faces of lysozyme crystals by Konnert et al. (1994).

Three-dimensional reconstruction based on Fourier filtering was carried out using the integrated program system ICE written by Hardt et al. (1996), running on an SGI 340 VGX. These programs were originally written for the evaluation and filtering of electron microscope images of periodic structures, but are entirely applicable to AFM images as well. The Fourier transform of the raw AFM image is first presented so that the user can choose indices for three noncolinear intensities. An appropriate lattice is computed and refined against the entire intensity distribution, and intensities are then measured within a specified radius of the points falling on the refined lattice.

Because of distortion in the AFM image as a consequence of sample instability, variation in tip force, or the influence of fluid, the images are subjected in ICE to an automated unbending process (Henderson et al., 1986) to improve uniformity. The intensities and their phases are then Fourier transformed a second time to produce a filtered image of a single unit cell, which is then expanded to produce an area of specified dimensions. Details of the program package are found in the paper by Hardt et al. (1996).

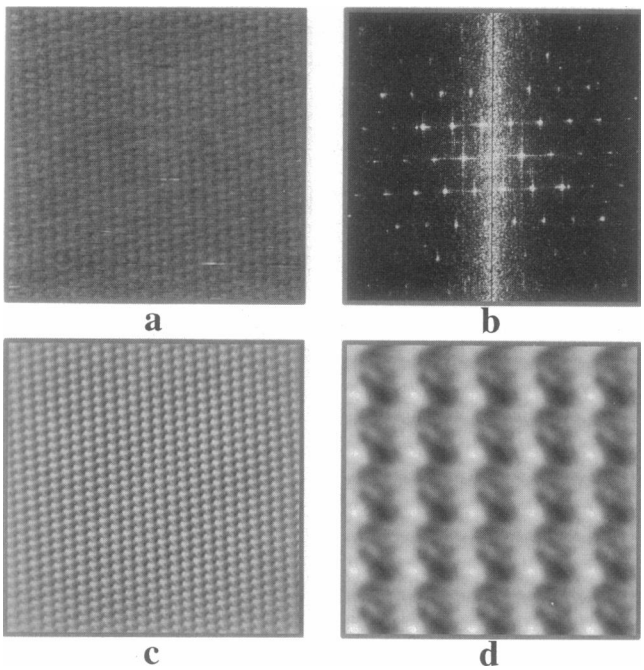

FIGURE 3 (*a*) A 300 × 300 nm^2 scan area, raw image of the surface of a rhombohedral crystal of canavalin, with space group R3, $a = b = c = 83$ Å, $\gamma = 111°$, and equivalent hexagonal unit cell parameters of $a = b = 136.8$ Å and $c = 75.7$ Å. (*b*) Its diffraction pattern, which has a resolution of about 12 Å. (*c*) Fourier-filtered image of *a*. The Fourier-filtered image of a smaller scan area (5 × 5 unit cells) is seen in *d*. Individual molecules are consistently visible in *a*, *c*, and *d*, and some molecular features are even beginning to emerge in *d*. Filtering was carried out using the program ICE.

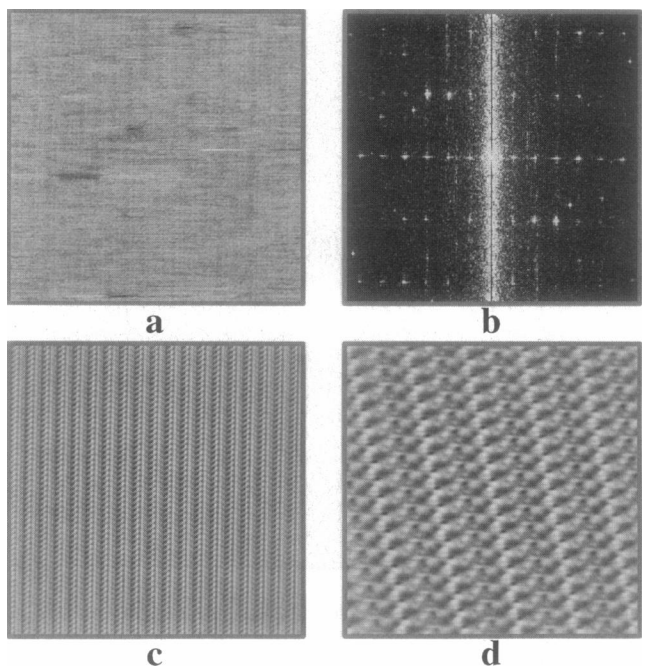

FIGURE 4 (*a*) A 250 × 250 nm^2 scan area, raw image of the (110) face of a tetragonal crystal of hen egg white lysozyme, with space group $P4_32_12$ and $a = b = 37.9$ Å and $c = 79.2$ Å. (*b*) Its diffraction pattern, which has a resolution of about 14 Å. (*c*) The corresponding Fourier-filtered image. (*d*) Fourier-filtered image of a small scan area (75 × 75 nm^2). The agreement of the image presented in *d* compares well with model images calculated by Konnert et al. (1994) using a tip-surface simulation approach. Filtering was carried out in this case using Digital Instrument provide software.

RESULTS

Figs. 2 *a*, 3 *a*, 4 *a*, 5 *a*, and Fig. 6, *a* and *c*, are direct, unaltered images of the five macromolecule crystals. Not only is lattice resolution evident, but, even in these raw images, individual protein or virus particles can, in some cases, be seen to be incorporated into the surface layers of their crystals. Fourier inversion of the images produces the two-dimensional diffraction patterns shown in Figs. 2 *b*, 3 *b*, 4 *b*, and 5 *b*. These were subsequently filtered and Fourier transformed a second time to produce the images seen in Figs. 2 (*c* and *d*) through 5 (*c* and *d*), and 6 (*b* and *d*).

Although less accurate than information provided by x-ray diffraction, cell dimensions of crystals and the likely number of molecules per asymmetric unit can be deduced from AFM images of macromolecular crystal surfaces. This depends on knowing the face of the crystal recorded and the crystallographic directions. From cell dimensions, features such as density and solvent content can be calculated (Matthews, 1968). In the thaumatin crystal in Fig. 5, for example, periodicities along the prominent rows and perpendicular to the rows, as measured from the AFM images, are 60 Å and 160 Å, respectively. These correspond to the *a* axis length (58.6 Å) and the dimension in the 101 direction (162.7 Å) deduced from x-ray diffraction. For this particular crystal, the difference of the AFM values from the "true" values determined by x-ray diffraction is ~2–3 Å, and the calculated unit cell volume difference is ~3%. For canavalin crystals seen in Fig. 3, the observed periodicity corresponds to the rhombohedral unit cell edge and is 81 Å, compared with the x-ray deduced value of 83 Å.

Although projections of some of the crystals perpendicular to the particular planes recorded here would exhibit orthogonal lattices and higher symmetry, as would the corresponding x-ray diffraction patterns, the images and diffraction patterns shown in Figs. 2–6 do not. This is because the surface of a crystal, in general, does not exhibit the same symmetry as the entire crystal, and usually the surface symmetry is low. This is particularly evident for the (110) face of lysozyme (space group $P4_32_12$) and the (101) face of thaumatin crystals (space group $P4_12_12$). For these, the diffraction patterns possess only a center of symmetry, due to Friedel's law, and the images themselves lack even that.

Of the crystals studied here, those of lipase, lysozyme, and thaumatin present potential space group ambiguities to the x-ray crystallographer. Preliminary x-ray diffraction analyses revealed that the lipase crystal had either space group $P6_1$ or $P6_5$, but could not determine which. X-ray diffraction photographs of thaumatin crystals and lysozyme crystals establish their space groups as being either $P4_12_12$ or $P4_32_12$, but again, do not permit discrimination between the two.

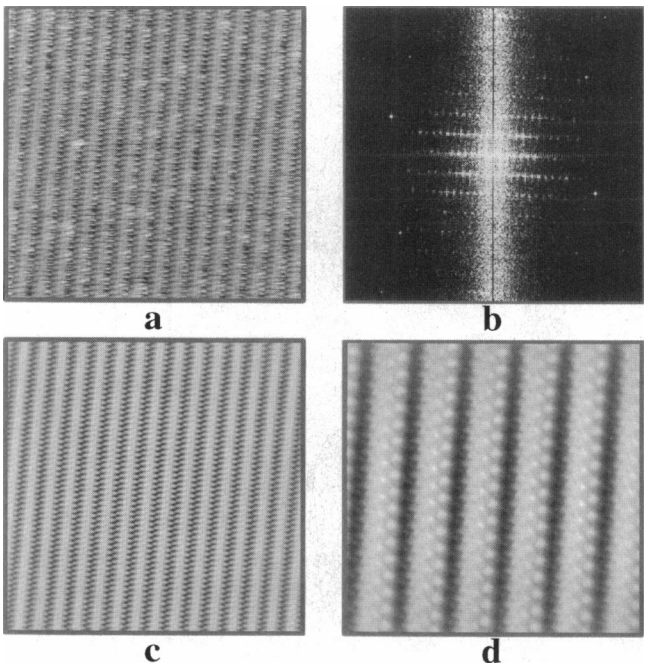

FIGURE 5 (*a*) An unprocessed image (scan area 300 × 300 nm^2) from the (111) face of a tetragonal crystal of the protein thaumatin, with space group $P4_12_12$ and $a = b = 58.6$ Å and $c = 151.8$ Å. (*b*) Diffraction pattern from a raw image with a resolution of about 10 Å. (*c*) Fourier-filtered image of *a*. (*d*) Fourier-filtered image of a small scan area (100 × 100 nm^2). The pattern seen in *d* can be resolved into aggregates of individual molecules that must, of course, be related by crystallographic symmetry operators. The image in *d* was in fact, derived from the diffraction pattern in *b* for this illustration. Filtering was carried out using Digital Instrument provide software.

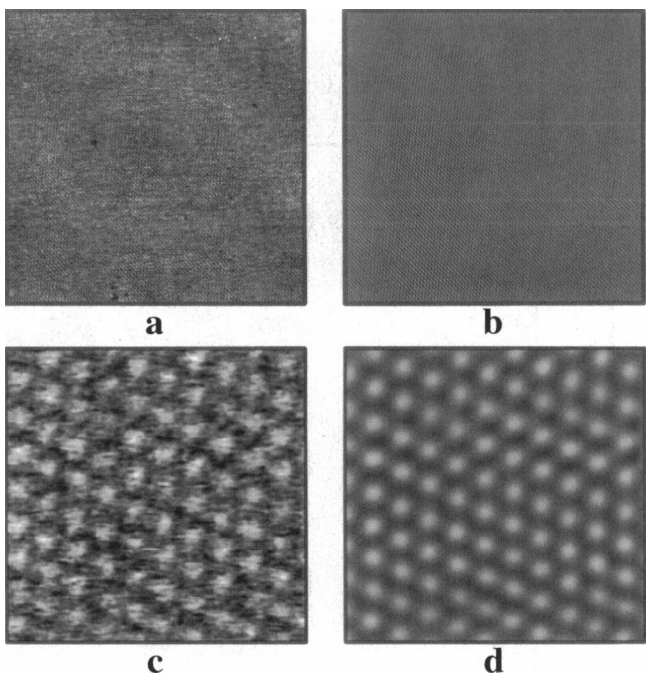

FIGURE 6 (*a* and *c*) Raw images of scan sizes 2 × 2 μm^2 and 210 × 210 nm^2, respectively, of the (111) face of a cubic STMV crystal of space group P23, with $a = b = c = 247$ Å. (*b* and *d*) Corresponding Fourier-filtered images of *a* and *c*. In all images, individual virus particles can be clearly seen composing the crystal lattice, but even in the Fourier-filtered images there are no indications of the icosahedral substructure of the virions.

Space group ambiguities can, and in the case of thaumatin did, result in significant complications (Ko et al., 1994). For structure determination by multiple isomorphous replacement, they produce an ambiguity in the configuration of the heavy atom constellation derived from Patterson maps, and in the assignment of proper sign to anomalous dispersion differences used in phasing. Space groups are sometimes resolved only by examining features such as helix chirality once the macromolecule's structure has been determined. In a molecular replacement structure determination, space group ambiguity leads to an uncertainty in interpretation of the translation function.

Fig. 2 contains images of the (100) face of a lipase crystal. Measurements of the dimensions from AFM images ($a = 145$ Å, $c = 79$ Å) are in good agreement with those established by x-ray diffraction ($a = 142.7$ Å, $c = 80.5$ Å). The orientation of the *c* axis is evident, as are individual molecules forming a helical array about *c*. Because height information preserves the third dimension, the helical array must be left-handed. The space group is, therefore, $P6_5$. This arrangement, deduced by inspection, can be verified by modeling the surface using spheres for the molecules, the known cell dimensions, and the alternative space groups. An example is shown for the lipase crystal in Fig. 7.

The situation with thaumatin is somewhat more difficult, as the (101) plane seen in the AFM image of Fig. 5 does not contain the *c* axis, which could be either 4_1 or 4_3. It is not evident by inspection what the chirality of the space group is. The appearance of the (101) faces of crystals with enantiomorphic space groups is different, however, and simulations of their structures can be used to resolve the ambiguity. In Fig. 8, for example, two kinds of surface models for thaumatin crystals are presented, both corresponding to the correct space group, $P4_12_12$.

The lipase crystal surface of Fig. 2 provides other crystallographic information. This crystal has two protein molecules in its asymmetric unit, if one assumes the calculated volume-to-mass ratio of $V_m = 3.12$ Da/A^3 (Matthews, 1968). Relative dispositions of two crystallographically independent molecules can, in general, be deduced from x-ray diffraction data only by successful application of molecular replacement techniques. From the AFM image, however, an estimate of the translation relating the molecular centers of two independent molecules can be obtained by direct measurement. Again, because height information is preserved, the translation is a true translation in three dimensions, not a projection on the surface plane. Noncrystallographically related lipase molecules form two consecutive, parallel, left-handed helices around the *c* axis, although the orientations of the molecules may be different with respect to the

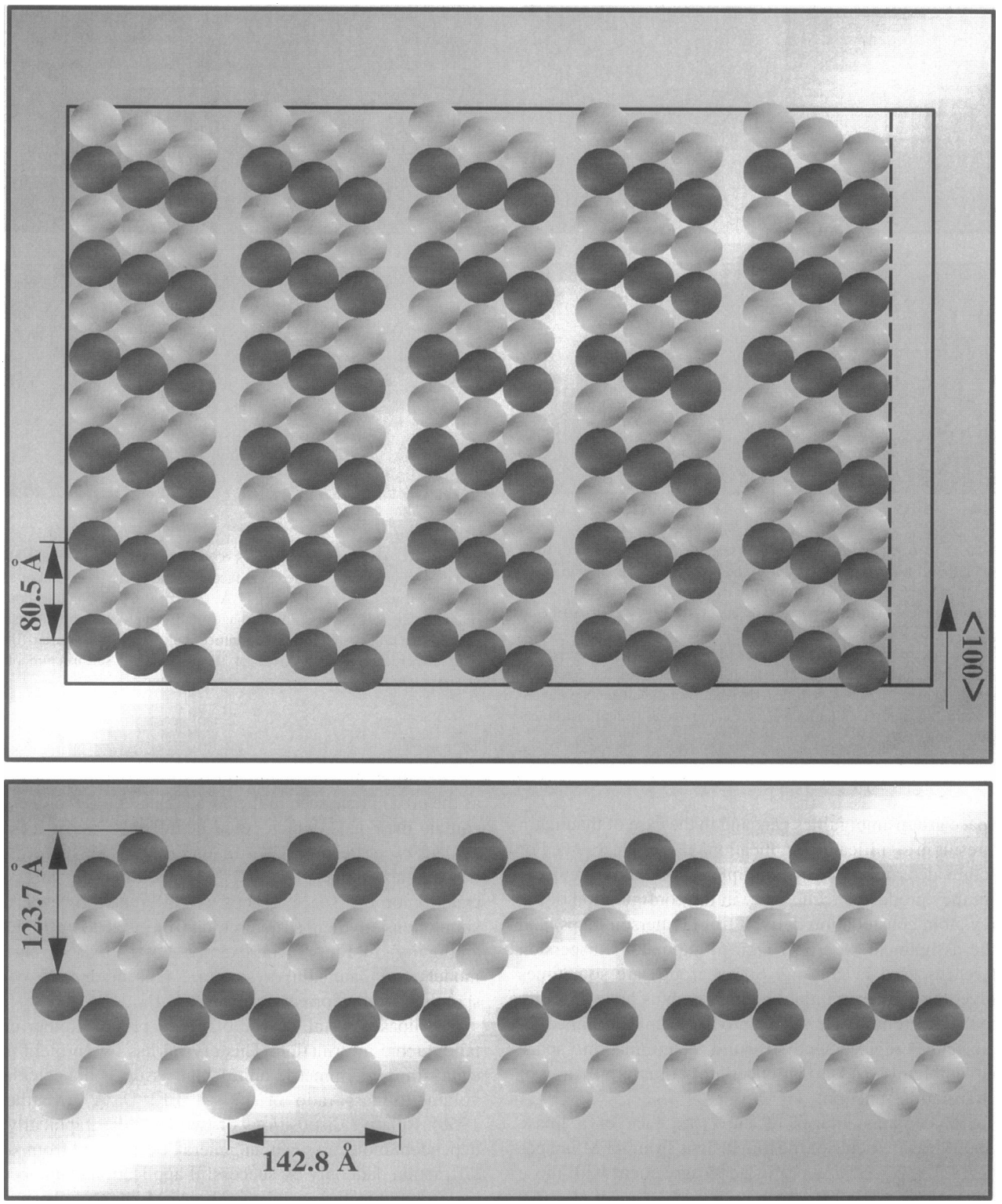

FIGURE 7 A computer simulation using the program ATOMS of the lipase crystal face, where each molecule is represented by a sphere, the shade of which indicates its height above the surface (*dark*, lowest; *light*, highest). (*a*) The major (100) face recorded by AFM in Fig. 2. (*b*) The orthogonal view (001), not recorded by AFM, which is along the *c* axis of the hexagonal prism.

crystallographic axes. In Fig. 2, dark- and light-colored molecules seen in Fig. 7 are not related by the 6_5 screw axis and, therefore, comprise an asymmetric unit. The vector between their centers has a length of about 40 Å, and from the packing simulations, would have components of approximately $x = 0.00$, $y = 0.00$, $z = 0.50$.

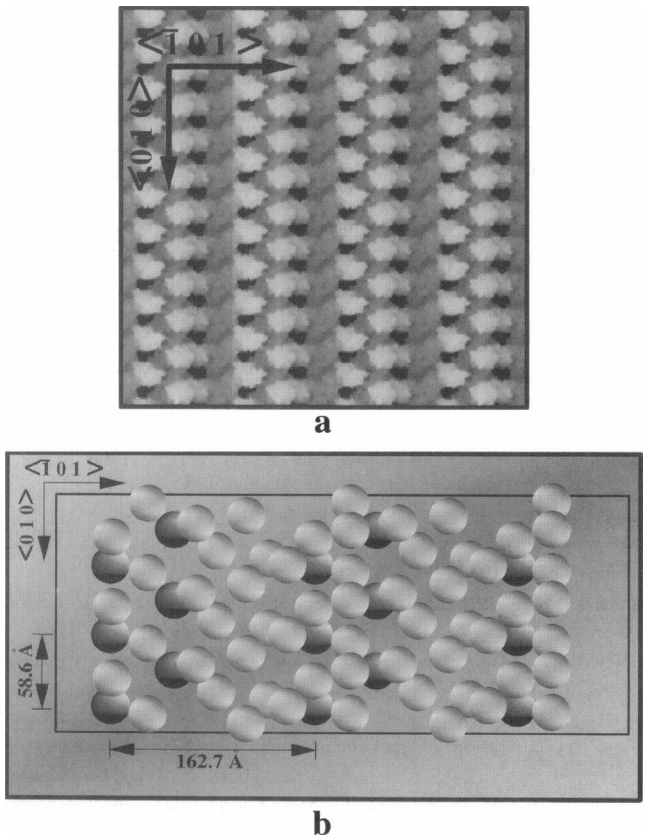

FIGURE 8 (*a*) Computer simulation of the (101) face of a tetragonal crystal of thaumatin produced using the procedures of Konnert et al. (1994). The shapes of the molecules, in their respective crystallographic orientations, are calculated from their crystallographic coordinates. The distribution of molecules on the surface is based on simulated scanning of an AFM tip over the computed surface. (*b*) Simulation of the packing of molecules, represented here only by spheres, on the (101) face of a tetragonal thaumatin crystal obtained using the program ATOMS. Lighter spheres are above and darker spheres below the mean height of the crystal surface. Comparisons of simulations such as these with AFM images of the corresponding crystal can in some cases resolve space group ambiguities.

The packing of molecules in the unit cell can also be estimated. In the $P6_5$ space group the z coordinate of the first molecular center is arbitrary. Simulation of the molecular surface with a range of values for the molecular centers and comparison with images of the crystal surface permit estimation and refinement of the other coordinates. From the packing model of the lipase crystal in Fig. 7, for example, one molecular center is at approximately 0.00, 0.00, 0.00, and the second is at about 0.00, 0.00, 0.50. This approach was shown to be valid for deducing the packing of molecules and the detailed modeling of the surface of thaumatin crystals in another study (Kuznetsov et al., manuscript submitted), and Konnert et al. (1994) have shown this as well for tetragonal lysozyme.

The surface of a cubic crystal of satellite tobacco mosaic virus is seen in Fig. 6. This crystal has space group P23, with cell dimensions of $a = b = c = 257$ Å. The centers of the virus particles in the unit cell (four in number) are, from the x-ray data alone, indeterminate. The lattice in Fig. 6 and the 180-Å center-to-center distances between particles imply that the virions are arranged in the cubic unit cell with pseudo-face-centered packing, with centers at 0,0,0 and 0,1/2,1/2. Thus packing considerations imposed by the distribution of particles on the surfaces of the cubic crystals, as visualized by AFM, were sufficient to obtain estimates of the viral centers (Malkin et al., 1995b).

Information of a different sort, not directly evident in most x-ray investigations of macromolecular crystals, can also be obtained. AFM images can supply a picture of the kinds of defects, at the lattice level, that are present in a crystal, and in many cases can even yield a quantitative measure of the defect density in the crystal. Discussed elsewhere (Malkin et al., 1996c), these are features that can impose limits on the size, mechanical properties, and the ultimate x-ray diffraction quality of crystals.

DISCUSSION

Atomic force microscopy, a relatively new and rapidly advancing technique, can be applied to macromolecular crystals, in some cases, to resolve ambiguities and obtain useful information that can accelerate and enhance x-ray diffraction analyses. Among the ways it can facilitate structural studies of crystals, are by resolving ambiguities in enantiomorphic space groups, providing information concerning the packing of molecules within the unit cell, yielding estimates of the relative dispositions of multiple molecules within an asymmetric unit, and, in the best of cases, supplying some picture of the gross structural features of the molecules themselves.

Although this latter benefit remains more a potential than an actual fact at this time, this is likely to change as the methodology improves, and as the study of macromolecular crystals with very large unit cells increases. Information of significant value might be obtained, for example, by application of AFM to the study of the surfaces of crystals of ribosomes and ribosomal subunits, very large viruses, large structural proteins, and multienzyme complexes. The methodology, furthermore, is appropriate for very small crystals with surfaces of no more than 30–50 μm^2, and crystals with unfavorable morphologies such as very thin plates. Thus information may, in some cases, be obtained for crystals of sizes and shapes inadequate for x-ray diffraction studies.

We would like to thank B. Shekunov, M. Schmidt, and M. Sherman for helpful discussions and A. Greenwood and R. Lucas for technical assistance.

This research was supported by the National Aeronautics and Space Administration and the Department of Energy.

REFERENCES

Alderton, G., and H. L. Fevold. 1946. Direct crystallization of lysozyme from egg white and some crystalline salts of lysozyme. *J. Biol. Chem.* 164:1–5.

Bustamante, C., and D. Keller. 1995. Scanning force microscopy in biology. *Physics Today.* 48:32–38.

Derewenda, Z. S., U. Derewenda, and G. G. Dodson. 1992. The crystal and molecular structure of the Rhizomuc or miehii triacylglyceride lipase at 1.9 Å resolution. *J. Mol. Biol.* 227:818–839.

Durbin, S. D., and W. E. Carlson. 1992. Lysozyme crystal growth studied by atomic force microscopy. *J. Cryst. Growth.* 122:71–79.

Durbin, S. D., W. E. Carlson, and M. T. Saros. 1993. In situ studies of protein crystal growth by atomic force microscopy. *J. Appl. Phys.* D26:B128–B132.

Hardt, S., B. Wang, and M. F. Schmidt. 1996. A brief description of ICE—the integrated crystallographic environment. *J. Struct. Biol.* 116:68–70.

Henderson, R., J. M. Baldwin, K. H. Downing, J. Lepault, and F. Zemlin. 1986. Structure of purple membrane from *Halobacterium halobium*: recording, measurement and evaluation of electron micrographs at 3.5 Å resolution. *Ultramicroscopy.* 19:147–178.

Hillner, P. E., S. Manne, P. K. Hansma, and A. J. Gratz. 1993. Atomic force microscopy—a new tool for imaging crystal growth processes. *Faraday Discuss.* 95:191–197.

Ko, T.-P., J. Day, A. Greenwood, and A. McPherson. 1994. The structures of three crystal forms of the sweet protein thaumatin. *Acta Crystallogr.* D50:813–825.

Ko, T.-P., J. D. Ng, J. Day, A. Greenwood, and A. McPherson. 1993a. X-ray structure determination of three crystal forms of canavalin by molecular replacement. *Acta. Crystallogr.* D49:478–489.

Ko, T.-P., J. D. Ng, and A. McPherson. 1993b. The three dimensional structure of canavalin from jack bean. *Plant Physiol.* 101:729–744.

Konnert, J. H., P. D'Antonio, and K. B. Ward. 1994. Observation of growth steps, spiral dislocations and molecular packing on the surface of lysozyme crystals with the atomic force microscope. *Acta Crystallogr.* D50:603–613.

Koszelak, S., J. A. Dodds, and A. McPherson. 1989. Preliminary analysis of crystals of satellite tobacco mosaic virus (STMV). *J. Mol. Biol.* 209:323–326.

Land, T. A., A. J. Malkin, Yu. G. Kuznetsov, A. McPherson, and J. J. DeYoreo. 1995. Mechanisms of protein crystal growth: an atomic force microscopy study of canavalin crystallization. *Phys. Rev. Lett.* 75: 2774–2777.

Larson, S. B., S. Koszelak, J. Day, A. Greenwood, J. A. Dodds, and A. McPherson. 1993. The three dimensional structure of satellite tobacco mosaic virus at 2.9 Å resolution. *J. Mol. Biol.* 231:375–391.

Malkin, A. J., Yu. G. Kuznetsov, W. Glantz, and A. McPherson. 1996a. Atomic force microscopy studies of surface morphology and growth kinetics in thaumatin crystallization. *J. Phys. Chem.* 100:11736–11743.

Malkin, A. J., Yu. G. Kuznetsov, T. A. Land, J. J. DeYoreo, and A. McPherson. 1995a. Mechanisms of growth for protein and virus crystals. *Nature Struct. Biol.* 2:956–959.

Malkin, A. J., Yu. G. Kuznetsov, and A. McPherson. 1996b. Incorporation of microcrystals by growing protein and virus crystals. *Proteins.* 24: 247–252.

Malkin, A. J., Yu. G. Kuznetsov, and A. McPherson. 1996c. Defect structure of macromolecular crystals. *J. Struc. Biol.* 117:124–137.

Malkin, A. J., T. A. Land, Yu. G. Kuznetsov, A. McPherson, and J. J. DeYoreo. 1995b. Investigation of virus crystal growth by in situ atomic force microscopy. *Phys. Rev. Lett.* 75:2778–2781.

Matthews, B. W. 1968. Solvent content of protein crystals. *J. Mol. Biol.* 33:491–502.

McPherson, A. 1982. The Preparation and Analysis of Protein Crystals. John Wiley and Sons, New York.

Ng, J. D., T.-P. Ko, and A. McPherson. 1993. Cloning, expression and crystallization of jack bean canavalin. *Plant Physiol.* 101: 713–728.

Yip, C. M., and M. D. Ward. 1996. Atomic force microscopy of insulin single crystals: direct visualization of molecules and crystal growth. *Biophys. J.* 71:1071–1078.